Cellular/Molecular

Target-Cell Specificity of Kainate Autoreceptor and Ca^{2+}-Store-Dependent Short-Term Plasticity at Hippocampal Mossy Fiber Synapses

Ricardo Scott,[1] Tatjana Lalic,[2] Dimitri M. Kullmann,[1] Marco Capogna,[2] and Dmitri A. Rusakov[1]

[1]Institute of Neurology, University College London, London WC1N 3BG, United Kingdom, and [2]Medical Research Council Anatomical Neuropharmacology Unit, Oxford OX1 3TH, United Kingdom

Presynaptic kainate receptors (KARs) modulate transmission between dentate granule cells and CA3 pyramidal neurons. Whether presynaptic KARs affect other synapses made by granule cell axons [mossy fibers (MFs)], on hilar mossy cells or interneurons, is not known. Nor is it known whether glutamate release from a single MF is sufficient to activate these receptors. Here, we monitor Ca^{2+} in identified MF boutons traced from granule cell bodies. We show that a single action potential in a single MF activates both presynaptic KARs and Ca^{2+} stores, contributing to use-dependent facilitation at MF–CA3 pyramidal cell synapses. Rapid local application of kainate to the giant MF bouton has no detectable effect on the resting Ca^{2+} but facilitates action-potential-evoked Ca^{2+} entry through a Ca^{2+} store-dependent mechanism. Localized two-photon uncaging of the Ca^{2+} store receptor ligand IP_3 directly confirms the presence of functional Ca^{2+} stores at these boutons. In contrast, presynaptic Ca^{2+} kinetics at MF synapses on interneurons or mossy cells are insensitive to KAR blockade, to local kainate application or to photolytic release of IP_3. Consistent with this, postsynaptic responses evoked by activation of a single MF show KAR-dependent paired-pulse facilitation in CA3 pyramidal cells, but not in interneurons or mossy cells. Thus, KAR–Ca^{2+} store coupling acts as a synapse-specific, short-range autoreceptor mechanism.

Key words: **synaptic plasticity; calcium [Ca]; presynaptic facilitation; kainic acid; Ca^{2+}-induced Ca^{2+} release; granule cell; hippocampus**

Introduction

Mossy fibers (MFs) represent an important excitatory projection to the hippocampus. Among their unusual properties is pronounced frequency-dependent (short-term) facilitation of transmission. However, this facilitation is more prominent at MF synapses on CA3 pyramidal cells than at MF–interneuron synapses (Toth et al., 2000). Furthermore, there are clear differences between the mechanisms of long-term plasticity at MF synapses on pyramidal cells and interneurons in the CA3 area (Pelkey et al., 2006). One consequence of this heterogeneity is that di-synaptic (feed-forward) inhibition of CA3 pyramidal neurons gives way to monosynaptic excitation during repetitive activity (Mori et al., 2004). However, the cellular mechanisms underlying these differences in short-term plasticity of MF synapses are incompletely understood.

At MF–CA3 pyramidal cell synapses, use-dependent facilitation of transmission has been shown to involve presynaptic kainate receptors (KARs) (Contractor et al., 2001; Lauri et al., 2001; Schmitz et al., 2001). A simple explanation for this phenomenon is that KARs activated by glutamate release from MFs themselves depolarize the presynaptic boutons or axons (Lauri et al., 2001; Kamiya et al., 2002; Nicoll and Schmitz, 2005). Indeed, axonal depolarization achieved by elevating the extracellular K^+ concentration can mimic synaptic facilitation associated with presynaptic KAR activation (Schmitz et al., 2001). This is consistent with the observation that partial inactivation of presynaptic K^+ channels due to repetitive spiking broadens action potentials, boosting presynaptic Ca^{2+} entry and therefore neurotransmitter release at these synapses (Geiger and Jonas, 2000). Furthermore, sub-threshold depolarization can successfully propagate between the somato-dendritic region and remote axonal segments in granule cells (Alle and Geiger, 2006; Scott et al., 2008), consistent with long-range electrotonic actions of presynaptic KARs in MFs. However, direct recordings from individual MF terminals in area CA3 show that transient local depolarization facilitates neurotransmitter release without a detectable increase in spike-evoked Ca^{2+} entry (Alle and Geiger, 2006; Scott et al., 2008). An alternative possible mechanism relating presynaptic KARs to use-dependent facilitation of neurotransmitter release from MFs involves Ca^{2+} release from internal Ca^{2+} stores (Liang et al., 2002; Lauri et al., 2003; Scott and Rusakov, 2006; Shimizu et al., 2008). However, a contribution of Ca^{2+} stores to presynaptic Ca^{2+} signals evoked in MFs by single or repetitive spikes remains controversial (Carter et al., 2002; Breustedt and Schmitz, 2004).

Hitherto, the roles of presynaptic KARs in MFs have been

Received June 25, 2008; revised Oct. 9, 2008; accepted Oct. 17, 2008.

This work was supported by Wellcome Trust, Medical Research Council (UK), European Union (PROMEMORIA LSHM-CT-2005-512012) and Human Frontier Science Program. We thank David Elfant for valuable comments on this manuscript.

Correspondence should be addressed to either of the following: Dmitri A. Rusakov or Ricardo Scott, Institute of Neurology, University College London, Queen Square, London WC1N 3BG, UK. E-mail: d.rusakov@ion.ucl.ac.uk or r.scott@ion.ucl.ac.uk.

DOI:10.1523/JNEUROSCI.2932-08.2008

 0270-6474/08/2813139-11$15.00/0

inferred from measurements of synaptic responses evoked by stimulating multiple axons. Such experiments may conceal variability among synapses, and also fail to distinguish between spillover-mediated interactions among synapses and a possible autoreceptor function in the strict sense, whereby neurotransmitter release from a single axon acts via receptors on the same presynaptic structure. To address these issues at higher resolution, we examined the role of KARs in modulating presynaptic Ca^{2+} kinetics and synaptic transmission at individual MF synapses traced from their parent granule cells. By combining patch-clamp electrophysiology with two-photon Ca^{2+} imaging and photolytic release of a Ca^{2+} store receptor ligand, we find that presynaptic KARs can be activated by glutamate released from a single axon, that such actions are specific to MF synapses on CA3 pyramidal cells (as opposed to interneurons or hilar mossy cells), and that they involve local Ca^{2+} stores.

Materials and Methods

Preparation and electrophysiology. All procedures involving animals were performed in accordance with UK Home Office regulations. Acute 300 μm slices from three- to four-week old male rats were transferred to a submersion-type recording chamber with temperature control (Scientific Systems Design) superfused with (mM): 124 NaCl, 2 KCl, 2 $CaCl_2$, 1 $MgCl_2$, 10 glucose, and bubbled with 95%/5% of O_2/CO_2. The internal solution contained (mM): 135 K methanesulfonate, 10 HEPES, 10 Na-Phosphocreatine, 4 $MgCl_2$, 4 NaATP, 0.4 NaGTP, and fluorophores as indicated; for minimal stimulation protocols, the solution was: 126 K-gluconate, 10 HEPES, 10 Na_2Phosphocreatine, 4 KCl, 4 Mg-ATP, 0.3 Na-GTP, and 0.5% biocytin. Unless specified otherwise, granule cells were held at −80 mV, and interneurons at −70 mV, and mossy cells or CA3 pyramidal cells at −65. In granule cells, orthodromic action potentials or escape currents recorded in, respectively, current- or voltage-clamp mode, were evoked by 1 or 2 ms depolarizing pulses (single or five at 20 or 50 Hz, as indicated); alternatively, 100 μs electrical stimuli were applied to *stratum lucidum* with a bipolar electrode. For minimal stimulation recordings, patch pipettes filled with ACSF were used as monopolar stimulation electrodes (intensities: 7–13 μA for pyramidal cells, 13–20 μA for interneuron and 6.5–12 μA for mossy cell recordings); experiments were performed at 34 ± 1°C. Recording sweeps (normally 500 ms long) were digitized at 5 kHz, every 30 s or 1 min, and analyzed off-line using Patchmaster (HEKA) and Igor Pro 5.05 (Wavemetrics). Unless indicated otherwise, the perfusion solution contained 5 μM CGP55845, 50 μM D-amino-phosphonovaleric acid (APV) and 100 μM picrotoxin. Receptor antagonists were purchased from Tocris Cookson, fluorescent probes were purchased from Invitrogen, and biocytin from Sigma. Where required, drugs were added at the following concentrations: 2,3-dihydroxy-6-nitro-7-sulfamoyl-benzo[f]quinoxaline-2,3-dione (NBQX; 25 or 50 μM), LY354740 (0.5 μM), SR95531 (5 μM), UBP302 (10 μM), GYKI53655 (20–50 μM), GYKI52466 (50–100 μM).

Minimal stimulation protocol. This protocol was applied as detailed previously (Kerr and Capogna, 2007). Briefly, the stimulus intensity was gradually decreased until a small all-or-none response was detected in the postsynaptic neuron, with numerous failures (supplemental Fig. S4*D*, available at www.jneurosci.org as supplemental material) identified as events less than three times the SD of the baseline current fluctuations. The failure rate was defined as the number of failures divided by the number of trials; the paired-pulse ratio (PPR) was calculated as the mean peak amplitude of the response to the second stimulus divided by the mean peak amplitude of the response to the first stimulus (with failures included as zero-responses). Minimal stimulation responses in interneurons showed failure rates consistent with those reported for EPSCs evoked in paired granule cell–basket cell recordings (Alle et al., 2001). To further verify the validity of our protocols, we performed several control experiments. To assess the potential contribution of *postsynaptic* non-AMPA (and non-NMDA) receptors to our EPSC measurements, we examined the effect of 50–100 μM GYKI52466, a selective AMPA receptor antagonist (Paternain et al., 1995), on EPSCs evoked in CA3 pyramidal neurons or mossy cells by MF stimulation. These responses were strongly reduced by GYKI52466, leaving a residual, small and slower synaptic current ($n = 5$) (supplemental Fig. S4*A*,*B*, available at www.jneurosci.org as supplemental material). Minimal-stimulation EPSCs were stable >20–30 min of recording (supplemental Fig. S4*C*, available at www.jneurosci.org as supplemental material), whereas the effects of UBP302 were seen within a few minutes of its application (supplemental Fig. S4*E*, available at www.jneurosci.org as supplemental material); this suggests that any contribution of synaptic rundown to the effect is unlikely. To further test that MFs were indeed stimulated, 0.5 μM LY354740, a selective agonist for group II mGluRs (Schoepp et al., 1999) expressed by MFs (Shigemoto et al., 1997), was applied in the end of experiment. This abolished the EPSCs recorded from CA3 pyramidal cells, mossy cells or interneurons ($n = 12$) (see an example in supplemental Fig. S4*C*, available at www.jneurosci.org as supplemental material). Data samples were compared using a Wilcoxon signed-rank test for nonparametric distributions.

Two-photon excitation fluorescence imaging. Imaging experiments were performed using a Radiance 2000 system (Zeiss-Bio-Rad) optically linked to a femtosecond laser MaiTai (SpectraPhysics) and integrated with visual-control patch-clamp (Rusakov and Fine, 2003). Dentate granule cells were voltage-clamped at −80 mV and loaded with the morphological tracer Alexa Fluor 594 and the high-affinity Ca^{2+} indicator Fluo-4 (200 μM, K_d ~350 nM). Imaging was performed as detailed earlier (Scott and Rusakov, 2006). Briefly, fluorophores were excited at 800 nm, with laser power adjusted for optimal emission detection. The axon was followed from the soma into *stratum lucidum* using the Alexa emission channel and the system was focused on the MF bouton of interest. Recording started when the baseline fluorescence in both channels (Alexa and Fluo-4) was stable; responses were recorded in line-scan mode at 500 Hz (500 or 1000 ms sweeps, inter-sweep interval 30 s or 1 min) and analyzed off-line. Action potentials were routinely evoked by 1 or 2 ms somatic voltage command pulses (alternatively, by extracellular stimuli). Image analysis was performed on stacks of stored line-scan images using in-house NIH Image macros. The transient Ca^{2+}-dependent fluorescence response to the first action potential $(\Delta F/F)_1$ was measured as $(\langle F\rangle - F_{rest})/F_{rest}$ where F_{rest} and $\langle F\rangle$ are the average fluorescence measured >100 ms before and 20 ms after the spike, respectively, with the background fluorescence (average brightness outside any stained structures) subtracted. To measure the second action-potential-evoked signal $(\Delta F/F)_2$, the corresponding F_{rest} value was averaged over the time interval of 15–30 ms before the second spike. To measure the total Ca^{2+} signal over five action potentials (at 20 Hz), $\langle F\rangle$ was calculated over the 250 ms interval after the first spike. False color tables, averaged images and line-scan traces averaged over 5–10 sweeps either from individual cells or among several cells were used for illustration purposes but all quantitative analyses used the original (gray level) pixel brightness values measured in individual line-scans. When comparing group means, statistical significance was tested with a paired *t* test (Gaussian data scatter) or a non-parametric Wilcoxon matched pairs test (non-Gaussian data scatter).

In pressure-pulse experiments, the ion-insensitive Alexa emission channel was used as a normalization reference to control for (small) mechanical disturbance during the pulse initiation. In most experiments, we reconstructed the axon trajectory using a collage of high-resolution Kalman-filtered z-stacks 15–20 μm deep, representing 10-scan average frames.

Estimated detection threshold for Ca^{2+} signals in giant MF boutons. In a recent study, we estimated that, using similar methods, a ~2% increase in the basal Ca^{2+} level should be detectable, corresponding to ~2 nM of equilibrated free Ca^{2+} (Scott et al., 2008). Assuming a ~1 μm^3 sampled bouton volume, this corresponds to a total entry of 100–200 Ca^{2+} ions (Scott and Rusakov, 2006).

Two-photon uncaging of the Ca^{2+} store receptor ligand IP_3. In the imaging system, a second excitation channel was arranged by separating the existing excitation/emission optical path with a 80/20 neutral density filter cube placed between the objective back aperture and the scanhead. This channel was optically linked to a second independently controlled MaiTai laser; triggering of the laser shutter system (~1 ms time constant)

was synchronized with electrophysiology and imaging. To adjust the uncaging beam focus, ensuring confocality with the main excitation-emission channel, we imaged fluorescence (excitation in the uncaging channel–emission in the imaging channel) using either ~2 μm thick filter paper stained with Alexa Fluor 594 (λ_x = 800 nm) or 1 μm fluorescence beads. The optics were adjusted to provide a ~3 μm wide focal excitation spot (average spread in *X-Y-Z*) in the center of the microscope field of view. Caged IP_3 [*D*-myo-inositol 1,4,5-triphosphate, P4(5)-(1-(2-nitrophenyl)ethyl) ester, tris(triethylammonium) salt, 400 μM; Invitrogen] was added to the intracellular solution together with the Ca^{2+} indicator Fluo-4 and the morphological tracer Alexa Fluor 594 (both excited in the main imaging channel at λ_x = 810 nm). Once the indicators equilibrated (> 1 h), the MF bouton of interest (or, in control experiments, the dendrite of interest) was traced from the granule soma and the IP_3 cage was excited, in two-photon mode, at λ_u = 720 nm (five 2 ms pulses 50 ms apart) while recording the local Ca^{2+} signal. Because the onset of the Ca^{2+} signal in response to IP_3 uncaging varied among recordings, we measured the maximal fluorescence response $(\Delta F/F)_{max}$ averaged over a 100 ms window over the peak fluorescence level post-pulse.

Post hoc *reconstruction of recorded cells.* Where necessary, after electrophysiological recordings, slices were sandwiched between two filter papers (cellulose nitrate membrane filters, 0.45 μm, Whatman International) and immersed in 4% paraformaldehyde and 15% saturated picric acid in phosphate buffer (PB, 0.1 M, pH 7.4) for at least 24 h. Then, slices were embedded in gelatin and re-sliced at 60 μm using a Leica VT 1000S vibroslicer. Sections were washed in TBS (0.9% NaCl, 0.05 M tris, pH 7.4) and incubated overnight at 4°C in a 1:100 solution of avidin-biotinylated horseradish peroxidase complex (Vector Laboratories) in TBS + 0.1% Triton X-100 (VWR International). Sections were further washed in TBS and Tris buffer (TB, 0.05 M, pH 7.4) before incubation in 0.5 mg/ml diaminobenzidine (DAB, Sigma) in TB. Hydrogen peroxide (0.01%) was the substrate for the peroxidase reaction, which was performed in TB. Sections were rinsed in TB, then PB and subsequently mounted on gelatin coated slides and left to air-dry overnight. Slides were incubated in 0.08% osmium tetroxide, washed in PB, dehydrated in graded ethanol (EtOH; 50%, 70%, 90%, 95% and 100% ×2), immersed in xylene and permanently mounted on slides. Neurons were reconstructed and traced from successive serial sections using a 63× objective and plotted using a motorized microscope stage and computerized video-capture system (Neurolucida; MicroBrightField). Three-dimensional reconstructions were then visualized using Neuroexplorer (MicroBrightField).

Results

Use-dependent facilitation of presynaptic Ca^{2+} signaling at individual MF – CA3 pyramidal cell synapses involves kainate autoreceptor-dependent activation of Ca^{2+} stores

We asked whether glutamate released by a single action potential in a single MF is sufficient to influence presynaptic Ca^{2+} signaling via KARs. Granule cells were recorded in whole-cell mode while two-photon microscopy was used to trace their axons into the CA3 area where giant MF boutons synapse on pyramidal cells (Fig. 1*A–B*). After initial dye equilibration, these boutons show remarkable stability of presynaptic Ca^{2+} kinetics, with no evidence of washout of endogenous Ca^{2+} buffers for 2–4 h (Scott and Rusakov, 2006). We isolated KARs using the AMPA receptor antagonist GYKI53655 (30 μM, with GABA and NMDA receptors also blocked) and examined whether subsequent KAR blockade with the AMPA/KAR antagonist NBQX (25–50 μM) affects presynaptic Ca^{2+} signals evoked by repetitive action potentials (at 20 Hz). To monitor short-term use-dependent plasticity of presynaptic Ca^{2+} responses, we used the paired-pulse ratio of the first two Ca^{2+} signals, PPR = $(\Delta F/F)_2/(\Delta F/F)_1$. Because this ratio is relatively insensitive to variations in evoked presynaptic Ca^{2+} entry or in the resting Ca^{2+} level among axons (supplemental Fig. S1, available at www.jneurosci.org as supplemental material), it provides a robust gauge of use-dependent plasticity of Ca^{2+} signaling across the population of boutons. NBQX had only an insignificant effect on the resting Ca^{2+} fluorescence F_{rest} (average change 8 ± 4%, n = 10). However, it profoundly decreased the PPR (by 39 ± 8%, $p < 0.002$, n = 10) (Fig. 1*C–F*). This decrease was due to a marked reduction in $(\Delta F/F)_2$ (by 29 ± 9%, $p < 0.007$, n = 10) whereas changes in $(\Delta F/F)_1$ were insignificant (the average amplitude in control and NBQX was, respectively, 29 ± 4% and 33 ± 4%, n = 10). This effect of the broad-spectrum AMPA-kainate receptor blocker implies that KARs contribute substantially to paired-pulse facilitation of presynaptic Ca^{2+} entry at giant boutons.

Next we asked whether the specific antagonist of GluK1-containing KARs UBP302 affects Ca^{2+} kinetics in giant MF boutons. Bath application of 10 μM UBP302 had qualitatively the same effect as NBQX, albeit smaller on average: the PPR was decreased by 26 ± 5% ($p < 0.01$, n = 6) (Fig. 1*G*; the difference between the effects of UBP and NBQX fell short of statistical significance). Although this result suggests that GluK1s contribute to the presynaptic KAR actions, pharmacological tools are not available to determine the role of other subunits, in particular GluR6 (Contractor et al., 2001; Lauri et al., 2001; Smolders et al., 2002; Breustedt and Schmitz, 2004).

To minimize exposure of the axon to laser scanning (Koester et al., 1999), we limited our experiments in individual boutons to 20–30 sweeps in line-scan mode. Although this restricted pharmacological testing to a single manipulation, the time course of the KAR blockade effect (Fig. 1*E*, supplemental Fig. S2*A*, available at www.jneurosci.org as supplemental material) and the comparison against a control group of boutons matching the timing of recording (n = 10; GYKI added from the start) indicated a robust KAR-dependent decrease in PPR (supplemental Fig. S2*B*, available at www.jneurosci.org as supplemental material). Furthermore, we detected a 26% difference ($p < 0.04$) in the absolute PPR values between two separate groups of giant MF boutons in CA3 area, one in baseline conditions (n = 8, no GYKI added) and one with NBQX added from the start (n = 11), again, with the timing of recording matched (supplemental Fig. S2*C*, available at www.jneurosci.org as supplemental material). Furthermore, application of the Ca^{2+} permeable KAR blocker philanthotoxin (PhTx, 3 μM) produced a similar effect (a decrease of PPR by 24 ± 6%, n = 6, $p < 0.01$; no changes in F_{rest}, supplemental Fig. S2*D*, available at www.jneurosci.org as supplemental material). This suggests that Ca^{2+}-permeable KARs contribute to facilitation (see below), consistent with the effect of PhTx on MF transmission to CA3 pyramidal cells reported by (Lauri et al., 2003).

These data thus argue that neurotransmitter released by a single synaptic discharge from one giant MF bouton in area CA3 is sufficient to activate local presynaptic KARs, facilitating subsequent spike-evoked presynaptic Ca^{2+} transients. This autoreceptor action is consistent with the three-dimensional arrangement of active zones and glial protrusions at these synapses, which allow significant spillover of released glutamate over a large area of the presynaptic MF membrane (Rollenhagen et al., 2007).

To determine whether an interaction between KARs and internal Ca^{2+} stores at these synapses (Lauri et al., 2003) could explain KAR-dependent modulation of evoked Ca^{2+} signaling, we tested the effect of depleting these stores with ryanodine (30–50 μM). Under baseline conditions, ryanodine decreased the PPR significantly (by 23 ± 4%, $p < 0.002$, n = 7) (Fig. 1*H*), similar to the effect of KAR blockade (Fig. 1*F,G*). The Ca^{2+} store IP_3-receptor blocker 2-aminoethoxydiphenyl borate (2-APB, 14 μM) had a similar, albeit smaller effect (PPR decrease: 14 ± 4%,

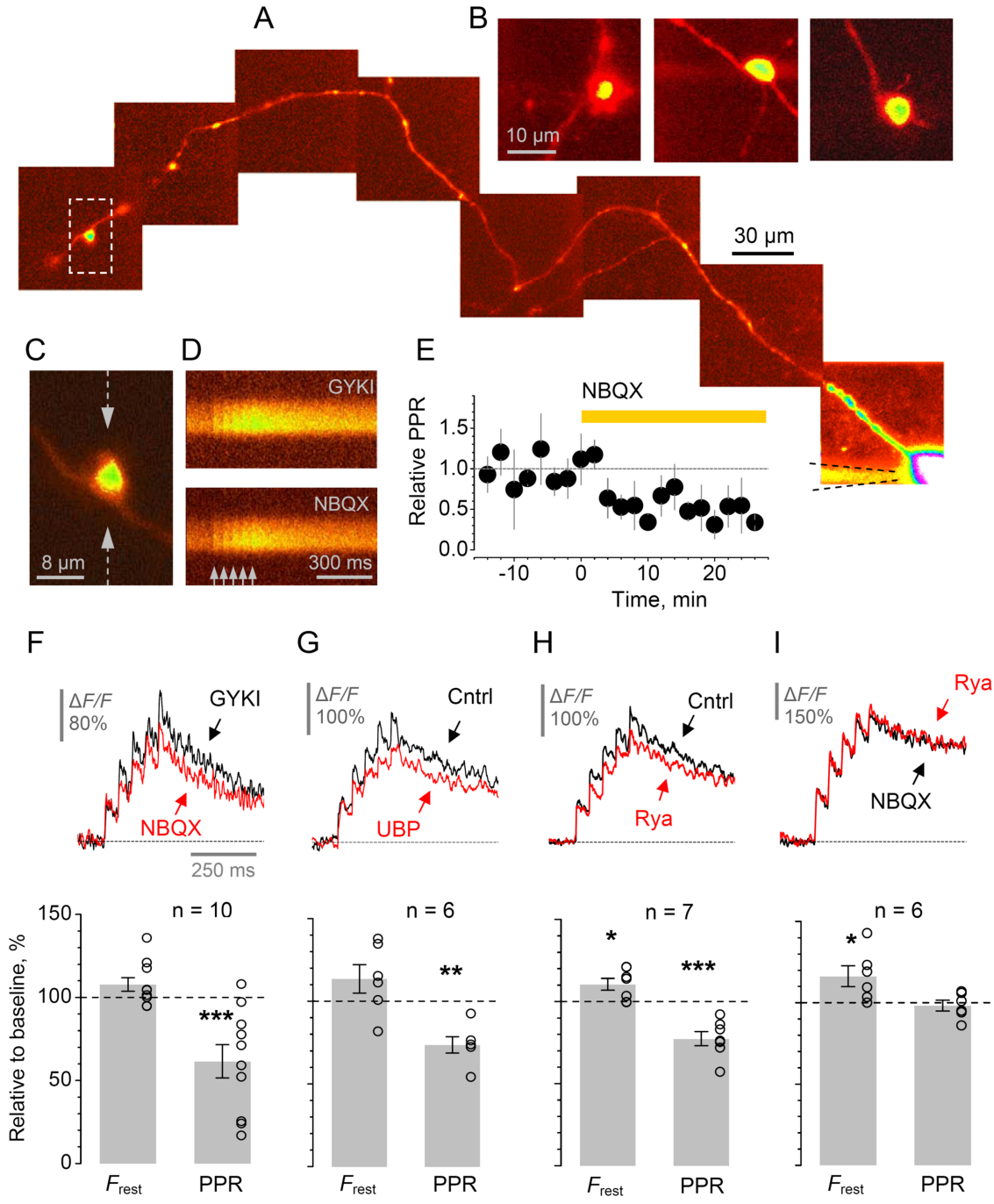

Figure 1. Kainate receptors modulate short-term plasticity of presynaptic Ca^{2+} entry at individual MF–CA3 pyramidal cell synapses involving rapid Ca^{2+} release from Ca^{2+} stores. ***A***, A granule cell axon traced from the soma (Alexa Fluor 594 emission, collage; see Materials and Methods); the CA3 giant bouton of interest is marked by a dashed frame and enlarged in ***C***. ***B***, Examples of giant MF boutons traced in area CA3, 300–700 μm from cell bodies. ***C–D***, In the giant bouton shown in ***C*** (also ***A***), five action potentials at 20 Hz (arrows) evoke clear Ca^{2+}-dependent fluorescence signals (line-scans in ***D***, Fluo-4 emission; 10-sweep average), in the presence of 20 μM GYKI53655 (GYKI), and after application of NBQX, as indicated. Line scan positioning is shown in ***C*** by dotted arrows. ***E***, The average time course for the effect of KAR blockade by NBQX (in the presence of GYKI, $n = 10$) on the paired-pulse ratio of action-potential-evoked Ca^{2+} responses, PPR $= (\Delta F/F)_2/(\Delta F/F)_1$. Error bars, SEM. ***F–G***, Blocking KARs with NBQX (***F***) or with 10 μM UBP302 (***G***) has little effect on the resting Ca^{2+} fluorescence F_{rest} but decreases PPR. Traces, characteristic line-scans (10-sweep average), as indicated. Bar plots, statistical summary: average change relative to control (open circles, individual experiments); $^*p < 0.04$; $^{**}p < 0.01$; $^{***}p < 0.005$. ***H–I***, Ca^{2+} store blockade by 50 μM ryanodine in control conditions reduces PPR (***H***) whereas the presence of NBQX completely occludes this effect (***I***). In both cases, ryanodine increases resting Ca^{2+} fluorescence F_{rest} (note that traces are baseline-normalized). $^*p < 0.03$; $^{***}p < 0.002$. Other notations are the same as in ***F–G***.

$n = 8$, $p < 0.01$) (supplemental Fig. S2*F*,*G*, available at www.jneurosci.org as supplemental material). If the contribution of Ca^{2+} stores to PPR regulation is controlled by local presynaptic KARs then blockade of KARs should occlude this contribution. Indeed, when we applied ryanodine in the presence of NBQX, the effect on PPR was undetectable (average change $-2 \pm 3\%$, $n = 6$) (Fig. 1*I*). A similar result was obtained in a complementary experiment, when NBQX was applied in the presence of ryanodine (PPR change: $3 \pm 3\%$, $n = 2$; data not shown). Intriguingly, blockade of Ca^{2+} stores increased the baseline Ca^{2+}-dependent fluorescence significantly, with or without NBQX (by $16 \pm 6\%$ and by $11 \pm 3\%$, respectively, $p < 0.03$ in both cases; note that

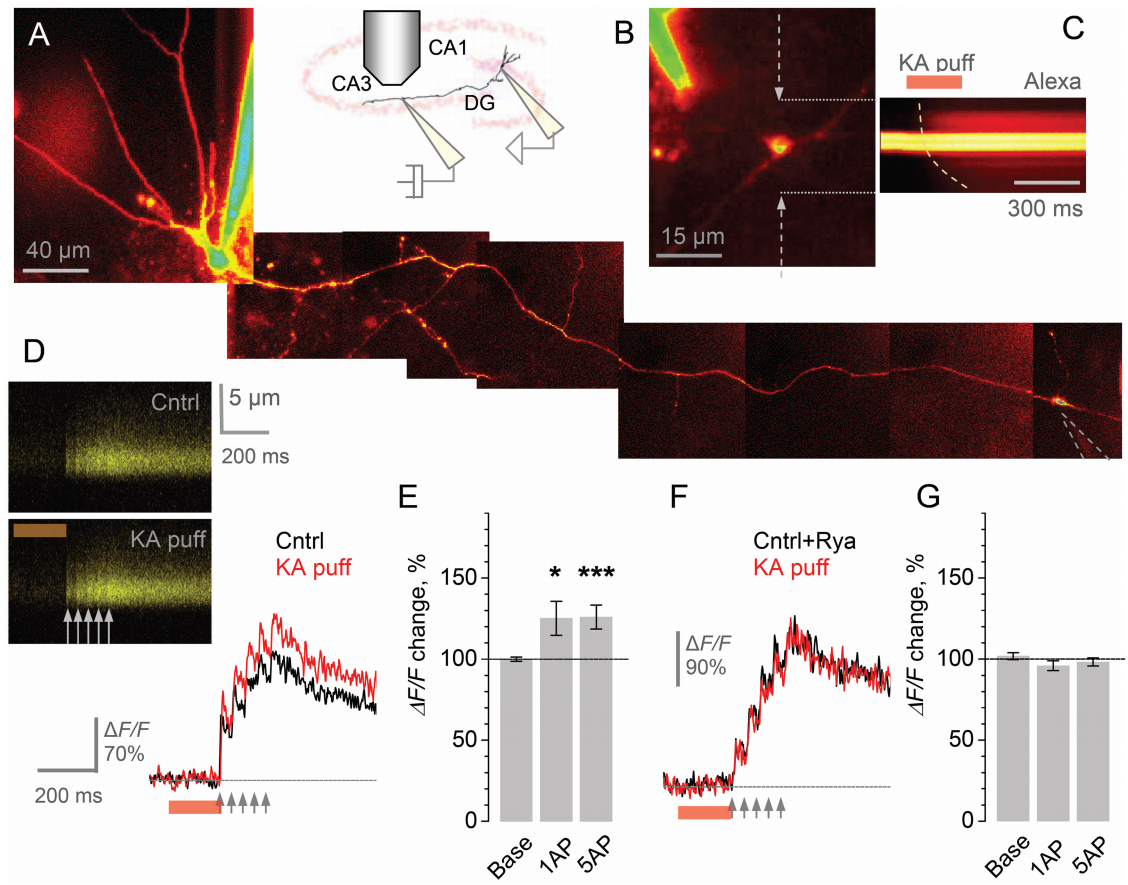

Figure 2. Direct (brief and local) application of kainate boosts action-potential-evoked Ca^{2+} entry in giant MF boutons in area CA3 whereas Ca^{2+}-store blockade abolishes this effect. ***A***, A granule cell axon traced from the soma (Alexa channel; patch pipette seen) with a pressure pipette (lightened area bordered by dotted lines) approaching a giant MF bouton in area CA3. Inset, a schematic illustrating the arrangement of a whole-cell and a pressure pipette in a slice with respect to the dentate gyrus (DG). ***B–C***, A characteristic experiment in which the pressure pipette approaches a giant bouton in CA3 (***B***). Kainate (100 μM) is ejected, together with Alexa Fluor 594 (2 μM), from the pipette using a 200 or 250 ms pressure pulse (line-scan in ***C***); the fluorescence transient reflects the pulse concentration profile overlapped with the bright bouton profile (a small, <1 μm, deflection corresponds to a mechanical/optical distortion during the pulse onset; dotted line, the apparent diffusion wave front). ***D***, Local pressure application of kainate has no effect on the baseline (resting) Ca^{2+} but increases action-potential-evoked Ca^{2+} entry in giant MF boutons in area CA3: a characteristic example of the baseline fluorescence and Ca^{2+} signals evoked by five action potentials (20 Hz, arrows) in control conditions (Cntrl) and during the kainate puff (KA puff; line-scans and color-coded traces shown; Fluor-4 channel; orange segment, kainate application pulse). ***E***, Statistical summary of experiments shown in ***D***. Bars, average change in the baseline presynaptic Ca^{2+}-dependent fluorescence (Base) and in the action-potential-evoked $\Delta F/F$ signals induced by the pulse of kainate (1AP and 5AP, Ca^{2+} responses to one and five action potentials, respectively); $*p < 0.04$; $***p < 0.005$. ***F–G***, Ca^{2+} store depletion with ryanodine (Cntrl+Rya) abolishes presynaptic effects of kainate application. A characteristic example and statistical summary are shown. Notation is as in ***D*** and ***E***.

such increases per se have little effect on the PPR, supplemental Fig. 1, available at www.jneurosci.org as supplemental material). This suggests that ryanodine-sensitive stores play a role in maintaining the low resting Ca^{2+} at these synapses (Scott and Rusakov, 2006) independently of KARs.

Facilitation of presynaptic Ca^{2+} signaling by direct activation of local KARs is mediated by Ca^{2+} stores

The finding that the blockade of KARs inhibits use-dependent presynaptic Ca^{2+} entry at giant MF boutons (see above) leads to the prediction that transient activation of local KARs should enhance action-potential-dependent Ca^{2+} transients. We tested this prediction by monitoring the effect of kainate applied directly and briefly to the imaged giant bouton just before evoking an action potential. This was achieved using a pressure-application pipette ($\sim$1 μm tip) positioned at a distance of 10–20 μm from a giant bouton traced in the CA3 area (Fig. 2*A–B*; the pipette was filled with bath solution containing 100 μM kainate, to account for a many-fold concentration drop in the tissue 10–20 μm away from the tip). The spatio-temporal profile of the extracellular pulse was monitored by imaging Alexa Fluor 594 (2 μM) also added to the application pipette solution (Fig. 2*C*, line-scan), as described previously (Rusakov et al., 2005). We therefore compared spike-evoked presynaptic Ca^{2+} signals between alternating trials that either did or did not include pressure application of kainate (Fig. 2*D*). In some experiments, possible mechanical artifacts of pressure application were controlled for by confirming that Ca^{2+} signals during the puff in the presence of NBQX was indistinguishable from that in control sweeps (average change in the basal fluorescence and the first $\Delta F/F$ were, respectively, $-0.8 \pm 3.4\%$ and $-6 \pm 6\%$, $n = 3$; data not shown). In contrast to the effects of KAR blockade (Fig. 1), kainate application increased Ca^{2+} signals evoked by either a single action potential or a train (five at 20 Hz) by, respectively, $25 \pm 10\%$ and $26 \pm 7\%$ ($p < 0.04$ and $p < 0.005$, $n = 9$) (Fig. 2*D*,*E*), with no effect on residual Ca^{2+} fluorescence (average change post-pulse relative to baseline: $0.0 \pm 1.3\%$, $n = 9$). The increase in $\Delta F/F$, however, was completely abolished in the presence of ryanodine (average change: $-4 \pm 3\%$ and $-2 \pm 3\%$, $n = 4$) (Fig. 2*F*,*G*), consistent with a critical role of Ca^{2+} stores in mediating the

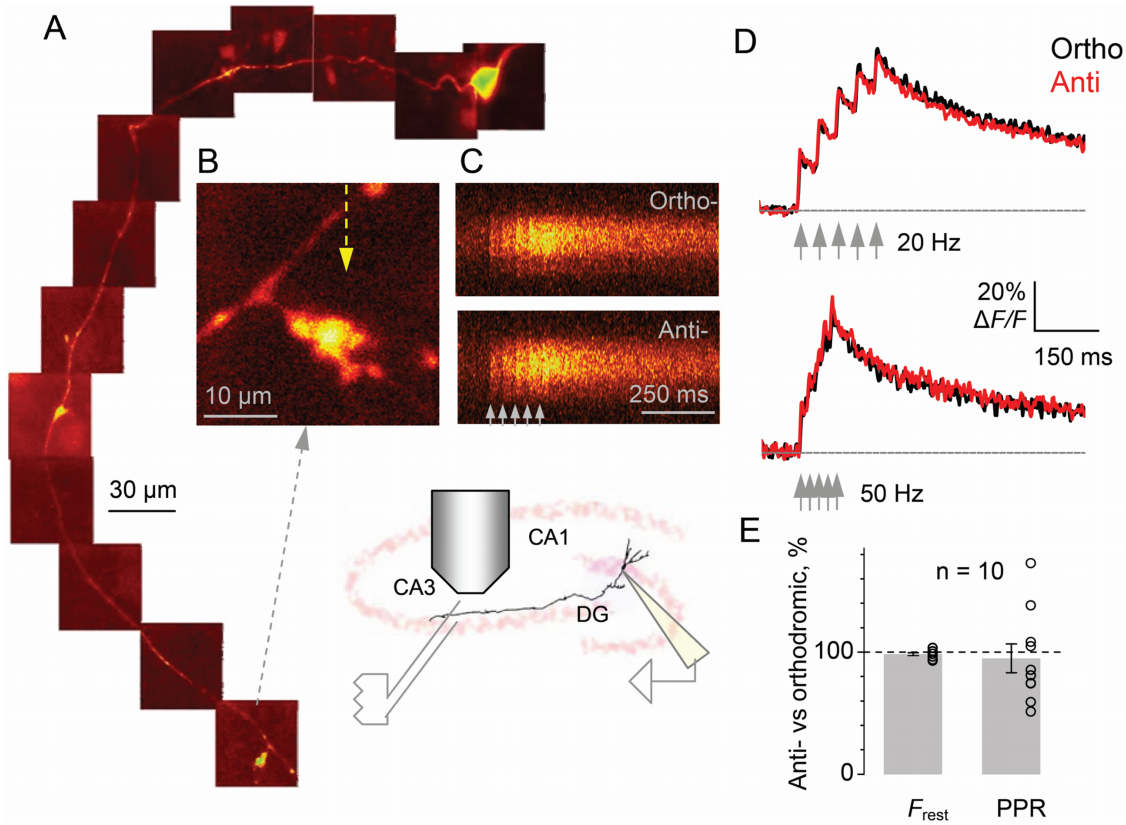

Figure 3. Presynaptic Ca^{2+} signaling in giant MF boutons (area CA3) and its short-term plasticity are not affected by activation of neighboring synapses. ***A–B***, A granule cell axon traced from the soma (Alexa Fluor 594 channel; collage in ***A***) showing the giant bouton of interest (expanded in ***B***); yellow arrow in ***B***, line scan position. ***C***, Ca^{2+}-dependent fluorescence (line-scans, Fluo-4 channel) evoked by five action potentials (20 Hz, arrows) in the bouton shown in ***B*** generated either at the soma (Ortho-; a 2 ms depolarization pulse applied through the patch pipette) or by local extracellular stimuli in area CA3 (Anti-), as indicated. Inset, a schematic of the experimental arrangement depicting positions of the whole-cell and stimulating electrodes. ***D***, The average time course of Ca^{2+}-dependent fluorescence in giant MF boutons evoked by five action potentials (20 or 50 Hz, as indicated) either orthodromically (black) or antidromically (red; mean normalized line-scan recordings for $n = 10$ cells are shown). ***E***, Statistical summary: comparison of intracellular orthodromic and extracellular antidromic stimulation. Average difference in resting fluorescence F_{rest} and paired-pulse ratio PPR $= (\Delta F/F)_2/(\Delta F/F)_1$ recorded in the antidromic with respect to orthodromic stimulation mode (open circles, individual experiments).

action of KARs. The finding that kainate application did not affect the baseline Ca^{2+} whereas the use-dependent facilitation of Ca^{2+} transients involved PhTx-sensitive, Ca^{2+}-permeable KARs (supplemental Fig. S2 *D*, *E*, available at www.jneurosci.org as supplemental material) raises the possibility that spatially restricted Ca^{2+}-dependent communication may take place between KARs and adjacent Ca^{2+} stores (see Discussion).

Short-term, use-dependent Ca^{2+} signaling in giant MF boutons does not depend on activity in neighboring synapses

High-frequency stimuli designed to evoke glutamate spillover have been reported to enhance MF – CA3 pyramidal cell transmission in a KAR-dependent manner and glutamate- and KAR-mediated interactions among multiple MFs have been proposed to impart associativity to MF long-term potentiation (Schmitz et al., 2003). The present results (Fig. 1) however indicate that a single action potential evoking neurotransmitter release from a single axon is sufficient to affect the response to a second action potential in a KAR-dependent manner. Does release from multiple neighboring synapses differentially affect Ca^{2+} signaling in an individual MF? To test this, we compared, in the same boutons, presynaptic Ca^{2+} signals in response to a train of five action potentials (at 20 or 50 Hz) evoked by somatic depolarization (therefore, in one cell) with those evoked by extracellular stimuli in *stratum lucidum* (Fig. 3*A–C*). In the latter case, the relatively long latency (3–4 ms) of antidromic spikes recorded at the soma confirmed that they were generated in the distal axon (Scott et al., 2008). Because the extracellular stimulating electrode was 20–50 μm from the imaged bouton and because *stratum lucidum* is densely packed with MFs, we reasoned that electrical stimuli that excited the imaged axon also activate neighboring axons. Indeed, once we finished recording in one cell, we could in some experiments patch a nearby granule cell and record antidromic action potentials using the same extracellular electrode, with no change in stimulus parameters or in the electrode position in *stratum lucidum* (data not shown). This implies that extracellular stimuli normally evoke glutamate release from multiple synapses in the vicinity of the imaged bouton. If short-term KAR-dependent facilitation of presynaptic Ca^{2+} signals shows associativity, this facilitation should be enhanced.

However, Ca^{2+}-dependent fluorescence transients showed no detectable difference when interleaved orthodromic and antidromic stimulation trains were compared: the changes in F_{rest} and PPR values during antidromic stimuli were, respectively, $-2 \pm 1\%$ and $-5 \pm 12\%$ relative to the values during orthodromic stimuli ($n = 10$) (Fig. 3*D*,*E*). This suggests that the associative property of KAR-dependent LTP (Schmitz et al., 2001) may be uncoupled from changes in presynaptic Ca^{2+} kinetics.

KAR-sensitivity of presynaptic Ca^{2+} signaling is specific to MF – CA3 pyramidal cell synapses

While most attention has been given to giant boutons on pyramidal cells in CA3, MFs also form morphologically similar bou-

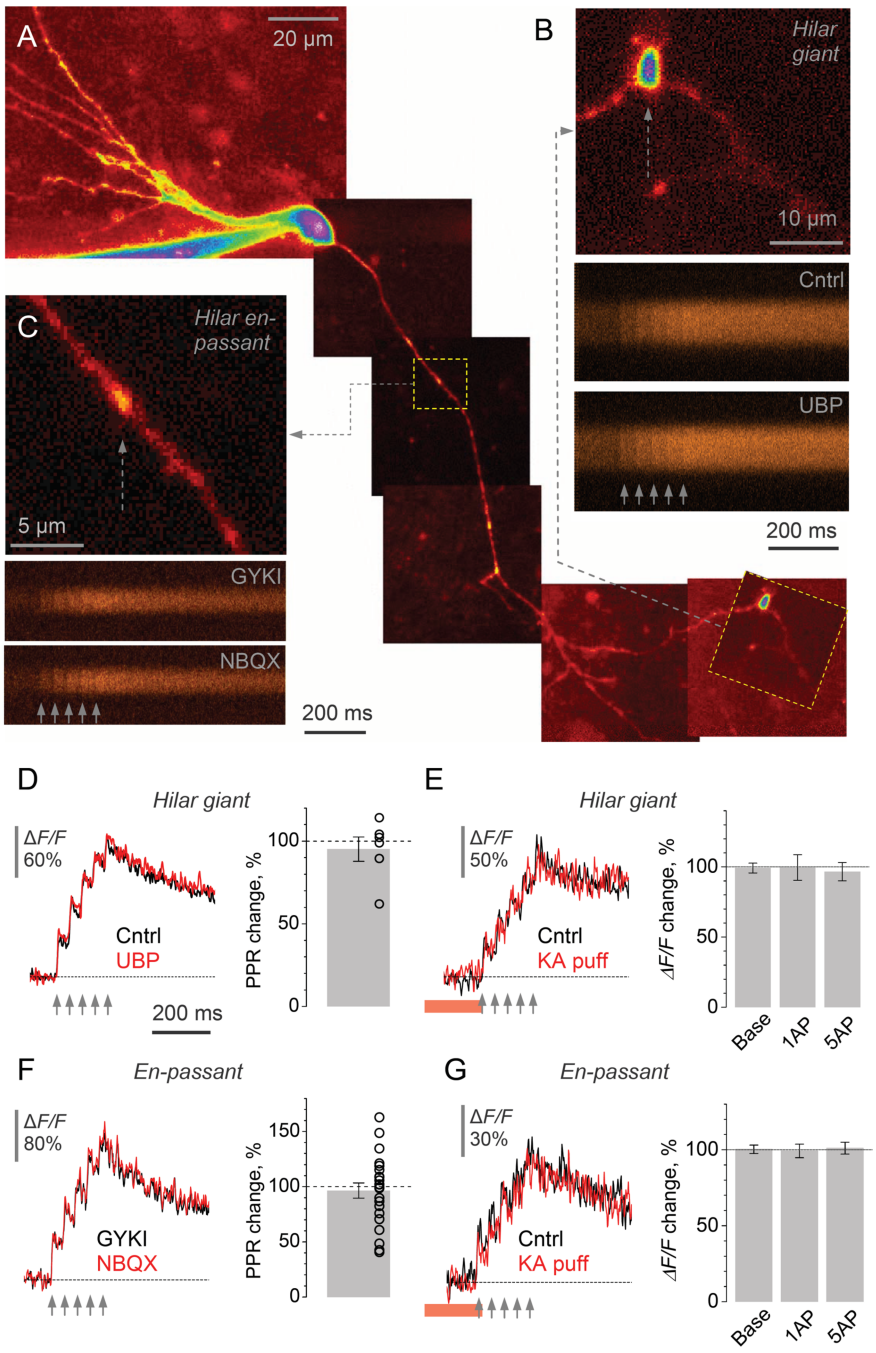

Figure 4. Presynaptic Ca^{2+} signaling at MF synapses on mossy cells or interneurons is insensitive to activation of KARs. ***A***, An initial segment of the granule cell axon including some collateral branches in the hilus (Alexa Fluor 594); an example. Dotted frames show a hilar en-passant bouton (representing a MF–interneuron synapse) and a characteristic hilar giant bouton (representing a MF–mossy cell synapse). ***B–C***, Examples of one-bouton recordings. Top, a close-up on the hilar giant bouton (***B***) or en-passant bouton (***C***) shown in ***A*** (Alexa channel). Bottom, line-scans (Fluo-4 channel) of presynaptic Ca^{2+} signals evoked by five action potentials (20 Hz, arrows) in baseline conditions (GYKI in ***B***, in the presence of GYKI53655; Cntrl in ***C***, control conditions) and following application of either UBP302 (***B***) or NBQX (***C***), correspondingly. ***D–E***, Characteristic line-scan traces and statistical summary for the effect of UBP302 (***D***) and of the kainate pressure puff (***E***) on presynaptic Ca^{2+} kinetics in giant MF boutons in the hilus; average PPR change is shown in *D* (open circles, individual experiments); average change in the baseline fluorescence response (Base) and in the $\Delta F/F$ amplitude following one (1AP) and five (5AP) action potentials is shown in *E*. Red segment, kainate puff; bars, average change; dots, individual experiments. ***F–G***, Characteristic line-scan traces and statistical summary for the effect of NBQX (***F***) and of the kainate pressure puff (***G***) on presynaptic Ca^{2+} signaling at en-passant MF boutons. See ***D–E*** and for notation.

tons on mossy cells in the dentate hilus, as well as smaller en-passant boutons and filopodial connections in synaptic contact with interneurons (Claiborne et al., 1986; Acsády et al., 1998; Toth et al., 2000; Pelkey et al., 2006). These synaptic types can be readily distinguished with two-photon microscopy (Fig. 4*A–C*; supplemental Fig. S3*A*, available at www.jneurosci.org as supplemental material).

We therefore repeated the experiments described above in en-passant boutons throughout the hilus and area CA3, as well as hilar giant MF boutons, mostly on MF collateral branches. In hilar giant boutons, KAR blockade had no detectable effect on PPR of Ca^{2+} transients (average change $-5 \pm 7\%$, $n = 6$) (Fig. 4*D*). Correspondingly, local pressure-application of kainate had no effect on the resting Ca^{2+} or Ca^{2+} entry in these boutons (the average change in the baseline fluorescence, 1-pulse and 5-pulse $\Delta F/F$ was, respectively, $0.8 \pm 3.5\%$, $0 \pm 9\%$, and $-3 \pm 7\%$, $n = 4$) (Fig. 4*E*). Neither was an effect of NBQX detected in small en-passant boutons formed by either the main or collateral MF branches (average change in PPR $-3 \pm 7\%$, $n = 22$) (Fig. 4*F*). Similarly, brief application of kainate near such boutons had no influence on presynaptic Ca^{2+} signaling (average change in the baseline fluorescence, 1-pulse and 5-pulse $\Delta F/F$ was, respectively, $0.3 \pm 2.8\%$, $-1 \pm 4\%$, and $1 \pm 3\%$, $n = 6$) (Fig. 4*G*).

Thus, in striking contrast to the effect of KARs on action-potential-dependent Ca^{2+} transients in giant MF boutons in CA3, no contribution of these receptors could be detected on synapses in the hilus. It is unlikely that this result was influenced by the whole-cell pipette prompting "washout" of Ca^{2+}-dependent mechanisms downstream of KAR activation: most giant hilar boutons (Fig. 4*A*) and a significant proportion of recorded en-passant boutons (supplemental Fig. S3*A*, available at www.jneurosci.org as supplemental material) occurred at distances from the soma similar to those for giant CA3 boutons that are sensitive to KAR activation. To test this further, we asked whether the effects of KAR blockade among synapses of the same type correlated with the distance from the somatic pipette. No such dependence was found (supplemental Fig. S3*B*,*C*, available at www.jneurosci.org as supplemental material).

Finally, we attempted to measure presynaptic Ca^{2+} kinetics in the thin filopodia of giant CA3 boutons, which represent synapses between MFs and interneurons in area CA3. However, the average fluorescence signals recorded in these small structures at a depth of up to 100 μm in the slice were too noisy to provide reliable assessment of KAR actions ($n = 8$, data not shown).

Functional presynaptic Ca^{2+} stores are specific to MF – CA3 pyramidal cell synapses

Does the target-cell specificity of the Ca^{2+} store-mediated KAR actions actually reflect an uneven distribution of Ca^{2+} stores

throughout the granule cell axon? To address this, we asked whether we could directly induce localized Ca^{2+} release from presynaptic stores at different presynaptic boutons throughout the granule cell axon. Because presynaptic Ca^{2+} signaling in giant MF boutons was equally sensitive to ryanodine (ryanodine receptor ligand, Fig. 1*F*,*E*) and 2-APB (IP_3 receptor blocker, supplemental Fig. S2*F*,*G*, available at www.jneurosci.org as supplemental material), it was likely that presynaptic Ca^{2+} store operation involved both receptor types (Verkhratsky, 2005). We therefore filled granule cells with caged IP_3 and tested whether its photolytic release (within a ~3 μm spot, in two-photon excitation mode; Materials and Methods) could induce local Ca^{2+} signals throughout the axon.

Indeed, in giant MF boutons traced into CA3, local uncaging of IP_3 induced a large Ca^{2+} transient (average $\Delta F/F$: 137 ± 57%, $n = 10$) (Fig. 5*A*). In contrast, no such responses could be detected in small en-passant boutons, in giant boutons in collateral axonal branches in the hilus, or in varicosities in the initial axon segment (average $\Delta F/F$, respectively: 6 ± 2%, 10 ± 3%, and 1 ± 2% $n = 19$, 13 and 9; a small residual effect was expected because escaped IP_3 could activate, on the scale of seconds, Ca^{2+} stores throughout a significant length of the axon) (Fig. 5*B*,*D*). This dichotomy could not be explained by the differential washout of the metabolic constituents in whole-cell mode. First, >50% of hilar (collateral branch) giant and en-passant boutons were recorded at a similar distance from the soma as the giant CA3 boutons: in these experiments, the average distances for all boutons in the three groups were, respectively, 238 ± 52 μm, 171 ± 34 μm and 337 ± 43 μm ($n =$ 13, 19, and 10). Second, photolytic release of IP_3 in proximal dendrites (average distance from the soma 158 ± 45 μm) showed a clear, albeit delayed, Ca^{2+} signal (average $\Delta F/F$: 57 ± 37%, $n = 22$) (Fig. 5*C*). Furthermore, in five experiments the patch pipette (containing 800 μM IP_3 and 400 μM Fluo-4) was withdrawn ~5 min post-break-in and the cell was allowed to recover; in these experiments, release of IP_3 induced no significant signals in en-passant axonal boutons while evoking a Ca^{2+} response in proximal dendrites (Fig. 5*D*, data included). These results are consistent with the hypothesis that the target-cell-specific action of presynaptic KARs on Ca^{2+} signaling in area CA3 giant MF boutons relies on selective occurrence of Ca^{2+} stores at these boutons.

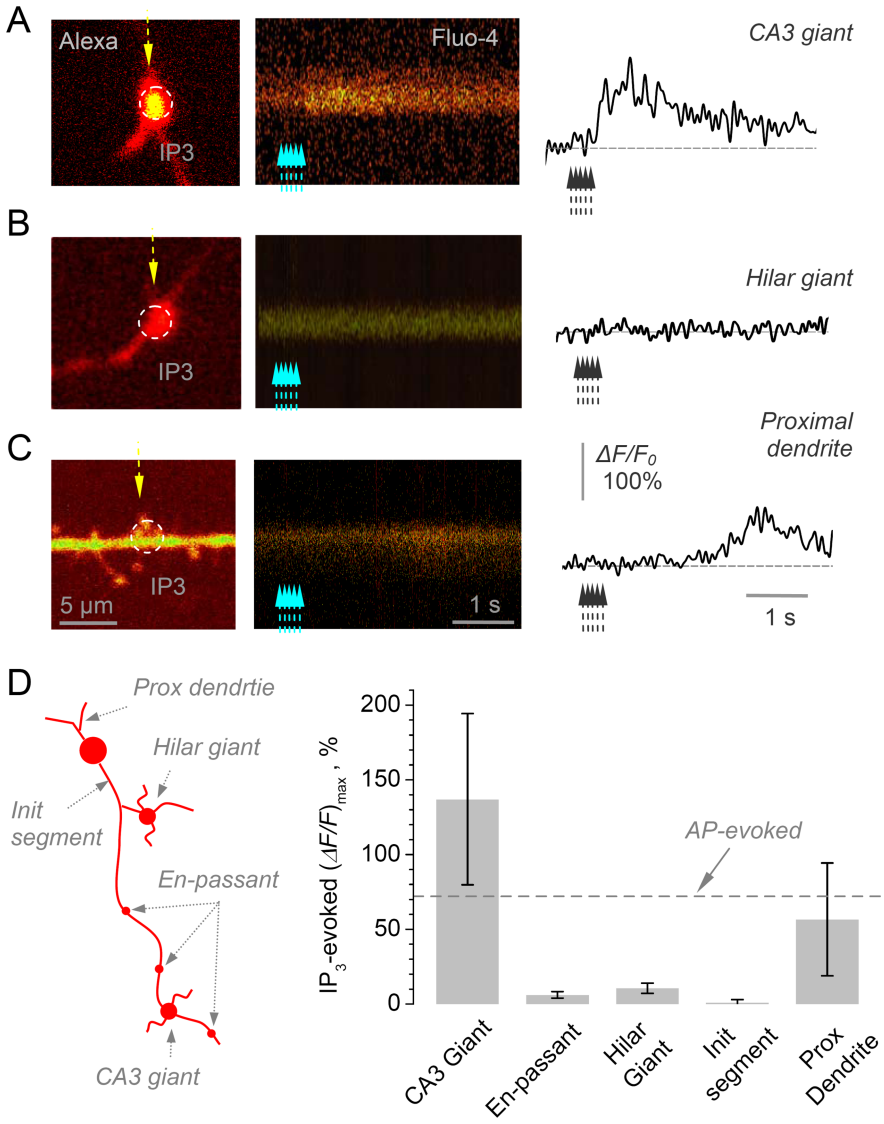

Figure 5. Local Ca^{2+} stores operate at giant MF boutons synapsing on CA3 pyramidal cells, but not in boutons representing synapses on mossy cells or interneurons. ***A***, A characteristic recording from a giant MF bouton in area CA3 showing the positioning of the uncaging spot (dotted circle, left panel; Alexa Fluor 594 channel) and line-scan imaging of Ca^{2+} responses (line-scan trace on the right and the corresponding plot; Fluo-4 channel) to five 1 ms uncaging pulses 50 ms apart ($\lambda_u = 720$ nm; indicated by dotted arrows). ***B***, A characteristic recording from a giant MF bouton in the hilus (collateral axonal branches). Other notation as in ***A***. ***C***, A characteristic recording from a granule cell proximal dendrite. The other notation is as in *A*; scale bars apply throughout ***A–C***. ***D***, Summary of IP_3 uncaging experiments including those shown in ***A–C***. Left diagram depicts characteristic sites of uncaging/Ca^{2+} signal recording in dentate granule cells. Bar graph, the average $(\Delta F/F)_{max}$ Ca^{2+} in response to local IP_3 uncaging at different locations as depicted on the left. Average values, CA3 giant boutons: 137 ± 57% ($n = 10$), en-passant MF boutons: 6 ± 2% ($n = 19$), giant MF boutons in collateral hilar branches: 10 ± 3 ($n = 13$), initial axonal segment varicosities: 1 ± 2% ($n =$ 9), proximal dendrites: 57 ± 37 ($n = 22$). The last two groups include five experiments in bolus loading conditions, with patch pipette removed 5 min after break-in. Dotted line (AP-evoked) indicates average action-potential-evoked Ca^{2+} response in area CA3 giant MF boutons, shown for comparison.

Presynaptic KARs facilitate glutamate release at MF synapses on CA3 pyramidal cell, but not mossy cells or interneurons

To relate the observed relationship between KARs and presynaptic Ca^{2+} signaling to neurotransmitter release at the respective synapses, we monitored EPSCs evoked by minimal stimulation of MFs in CA3 pyramidal cells, hilar interneurons and mossy cells (Jonas et al., 1993; Domenici et al., 1998; Lysetskiy et al., 2005; Kerr and Capogna, 2007). We routinely filled the recorded cells with biocytin and identified them *post hoc* (Kerr and Capogna, 2007). Postsynaptic responses recorded in these conditions displayed a significant proportion (>50%) of failures (Fig. 6, traces). We verified that the selective group II mGluR agonist LY354740 (0.5 μM) abolished evoked responses at the end of experiments, consistent with the sensitivity of MF-evoked transmission to this drug (supplemental Fig. S4*C*, available at www.jneurosci.org as supplemental material).

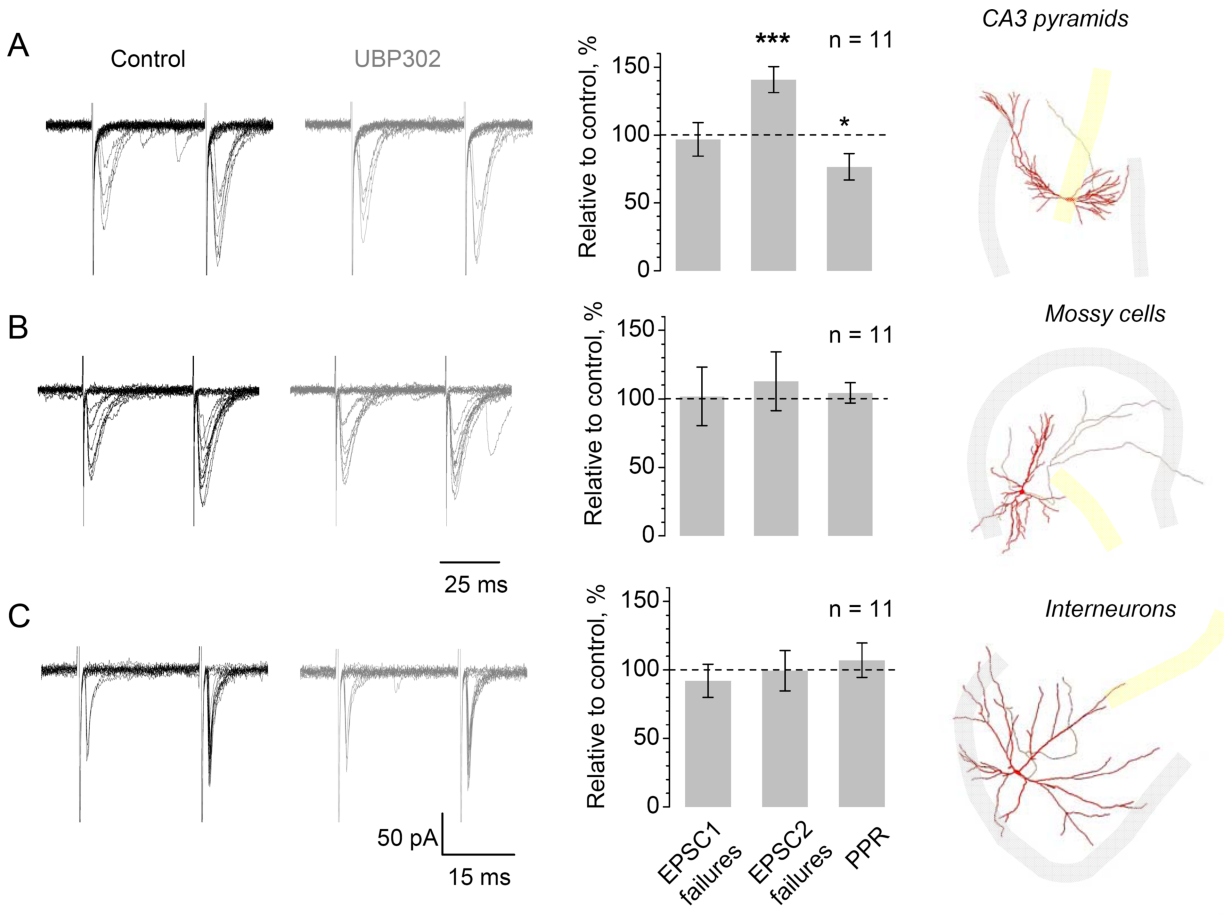

Figure 6. Presynaptic KARs contribute to short-term plasticity of EPSCs evoked by single-MF stimulation in CA3 pyramidal cells, but not in mossy cells or interneurons. ***A***, Left, one cell example: characteristic traces of minimal stimulation EPSCs evoked by paired stimuli (20 Hz) in CA3 pyramidal cells, in control conditions (black) and following application of UBP302 (10 μM, gray), as indicated. Graph, the effect of UBP on the failure rate of first response (EPSC1), second response (EPSC2) and on PPR (EPSC2/EPSC1 for average amplitudes including failures). See text and supplemental Fig. S4, available at www.jneurosci.org as supplemental material, for controls verifying the minimal stimulation protocol and the identity of MFs. See supplemental Table S1 for the numerical data summary, available at www.jneurosci.org as supplemental material. Right, an example of a CA3 pyramidal cell reconstructed *post hoc* (red and gray lines indicating dendrites and the axon, respectively); shaded area, granule cell (gray) and pyramidal cell (yellow) layers. *$p < 0.03$; ***$p < 0.001$. ***B–C***, No effect of KAR blockade on the release probability and short-term plasticity of minimal-stimulation EPSCs in mossy cells (***B***) and interneurons (***C***). Right (image) panels, examples of a mossy cell (***B***) and hilar interneuron (***C***) reconstructed *post hoc*. The notation is otherwise as in ***A***.

We evaluated the neurotransmitter release probability, and its short-term plasticity, by directly calculating the number of failures in a classical paired-pulse minimal stimulation paradigm (at 20 or 40 Hz). Under baseline conditions, the failure rates for the second-pulse EPSCs (EPSC2) were generally lower than those of the first-pulse responses (EPSC1) in all three classes of neurons (supplemental Table S1, available at www.jneurosci.org as supplemental material). In CA3 pyramidal cells, blockade of KARs with UBP302 increased the failure rate for the second EPSC by 41 ± 9% ($p < 0.001$, $n = 11$), and evoked a 24 ± 9% decrease of PPR (EPSC2/EPSC1 including failures; $p < 0.03$), with no effect on the basal release probability (change in the EPSC1 failure rate −3 ± 11%, $n = 11$) (Fig. 6*A*; see supplemental Fig. S4*E* for the time course of effect, available at www.jneurosci.org as supplemental material). In our recording conditions, presynaptic Ca^{2+} entry to giant MF boutons in area CA3 relates to EPSCs in CA3 pyramidal cells with a power of 2.5 ± 0.2 (Scott et al., 2008). Therefore, the observed increase in the second-pulse EPSC failures (above) could be fully explained by the blockade of the KAR-mediated facilitation of presynaptic Ca^{2+} transients at these synapses (Fig. 1). Strikingly, the same protocol produced no effects on average EPSC2 failure rates or PPR values measured in mossy cells or in interneurons (Fig. 6*B*,*C*).

These results are thus in full agreement with the Ca^{2+} imaging data, implying that presynaptic KARs contribute to use-dependent facilitation of neurotransmitter release specifically, if not exclusively, at MF–CA3 pyramidal cell synapses. Consistent with this difference, the baseline PPR of EPSCs recorded in CA3 pyramidal cells (3.21 ± 0.12, $n = 17$; six cells in control conditions were added) was higher than that recorded in interneurons (1.73 ± 0.21, $p < 0.05$, $n = 11$) or in mossy cells (2.13 ± 0.06, $p < 0.07$, $n = 17$; six cells in control conditions were added). This heterogeneity is particularly noteworthy with respect to morphologically similar giant MF boutons in area CA3 and in the hilus representing two different synaptic targets, pyramidal cells and mossy cells (Claiborne et al., 1986; Acsády et al., 1998; Henze and Buzsáki, 2007). Interestingly, blockade of KARs appears to abolish this heterogeneity (supplemental Table S1, available at www.jneurosci.org as supplemental material), suggesting that the KAR-dependent facilitation mechanism could explain differences in the degree of short-term plasticity among these three synaptic types.

Discussion

The principal findings of this study are as follows. First, a single action potential in a single MF bouton appears to be sufficient to activate presynaptic KARs, thus contributing to short-term use-

dependent facilitation of presynaptic Ca^{2+} entry in the same bouton. Ca^{2+} stores, which have been previously reported to contribute to short-term facilitation of transmission at MF synapses (Lauri et al., 2003), mediate the effect of KARs on Ca^{2+} signaling in giant MF boutons in area CA3. Second, use-dependent Ca^{2+} signaling at these boutons can be facilitated by direct activation of local KARs, but does not depend on glutamate release from multiple axons. These findings thus indicate an autoreceptor role of KARs more precisely. Finally, we found that other synapses formed by MFs do not show the same KAR-dependent mechanism of short-term facilitation. This target-cell specificity is fully consistent with the effects of blocking presynaptic KARs on short-term plasticity of EPSCs.

The mechanisms underlying the marked use-dependent plasticity of MF transmission have been intensely debated. Among the principal experimental difficulties lies the fact that MFs form synapses on several distinct cell targets. Therefore, pharmacological manipulations which affect modulatory mechanism(s) expressed at one specific type of MF connections potentially bias experimental observations of the MF circuitry as a whole. Understanding the principles of target-cell dependent modulation of MF transmission is further complicated by long-range electrotonic influences propagating throughout MFs (Alle and Geiger, 2006) and potentially by rapid recycling and trafficking of the presynaptic receptors involved (Hirbec et al., 2003). In addition, the complex trajectory of MFs (Claiborne et al., 1986; Acsády et al., 1998) implies that the slice cutting angle determines which section of MFs remains intact in the slice (Scott and Rusakov, 2006). These factors, together with potential differences in KAR subunit composition among experimental rodent species, could explain, at least partly, why we and others (Bortolotto et al., 1999; Lauri et al., 2001, 2003) have found a substantial contribution of GluK1-containing KARs to use-dependent facilitation of MF transmission (see above) whereas other groups have reported no such influence (Contractor et al., 2001; Breustedt and Schmitz, 2004; Pinheiro et al., 2007).

However, the aim of the present study was not to resolve the debate over the subunit identity of MF KARs but to establish the principles of synapse-specific actions of presynaptic KARs in MFs. By applying a single-synapse approach, we have shown that a single synaptic discharge in a single giant MF bouton in the CA3 area facilitates spike-evoked presynaptic Ca^{2+} entry in a KAR-dependent and Ca^{2+} store-dependent manner. Intriguingly, we found that the KARs involved are PhTx sensitive and therefore Ca^{2+} permeable (supplemental Fig. S2*D*,*E*, available at www.jneurosci.org as supplemental material). At the same time, however, direct local application of kainate to giant MF boutons had no detectable effect on the baseline Ca^{2+} level while promoting a Ca^{2+} store-dependent increase in evoked Ca^{2+} signals (Fig. 2). Given the finite Ca^{2+} detection threshold in our imaging experiments (Materials and Methods) these observations suggest that presynaptic KARs may have a privileged, spatially restricted coupling to local Ca^{2+}-stores and that this coupling may prime these stores, enabling them to discharge upon action potential arrival.

In contrast, MF synapses on interneurons or mossy cells show, on average, no involvement of presynaptic KARs in activity-dependent modulation of presynaptic Ca^{2+} signaling or release probability. We cannot fully exclude the possibility that the heterogeneity of mossy cells and interneurons synapsed by MFs in the hilus (Halasy and Somogyi, 1993; Jinno and Kosaka, 2003) conceals KAR-sensitivity for some cell targets beyond the experimental sample.

The present study defines the properties of the autoreceptor action with regard to MF KARs by showing that the release of glutamate from a single MF activates KARs expressed by the same fiber (Fig. 1), whereas stimulation of multiple fibers has no additional effect (Fig. 3). Although the term "autoreceptor" has been used with regard to MF KARs to reflect modulation of release of a neurotransmitter by that same neurotransmitter, our observations clarify the autoreceptor principle in this circuitry in the stricter sense. While abundant evidence exists for modulation of MF transmission by other presynaptic receptors (Lanthorn et al., 1984; Weisskopf et al., 1993; Manzoni et al., 1995; Kamiya et al., 1996; Simmons, 2002; Ruiz et al., 2003), previously it has not been possible to detect the action of agonists released from individual axons, in a "true" autoreceptor mode.

We also demonstrated that action potential dependent presynaptic Ca^{2+} release from Ca^{2+} stores depends on the "conditioning" activation of local KARs (Fig. 2) and thus does not require any long-range signals, such as electrotonic depolarization, generated by the axon. In addition, because en-passant boutons that show no involvement of KARs in Ca^{2+} signaling often occur between giant MF boutons in area CA3 and the soma, the roles of KARs and Ca^{2+} stores in the MF–CA3 pyramidal cell transmission cannot be explained by propagation of somato-dendritic influences in granule cells. This conclusion is significant in the light of recent findings showing a substantial electrotonic influence of granule cell somatic depolarization on MF–CA3 transmission (Alle and Geiger, 2006).

Interestingly, depletion of Ca^{2+} stores by ryanodine elevates the background Ca^{2+} signal F_{rest} in giant MF boutons by 15–20% (Fig. 1*H*,*I*) which corresponds to an increase of the resting Ca^{2+} in these boutons by 30–40% (Scott and Rusakov, 2006). This increase remains unaffected in the presence of NBQX (Fig. 1*I*) thus placing presynaptic KARs upstream of Ca^{2+} stores. Furthermore, ryanodine application in the presence of KAR blockers has no effect on either the PPR of action-potential-evoked Ca^{2+} signals (Fig. 1*I*) or the PPR of EPSCs in CA3 pyramidal cells (Lauri et al., 2003), suggesting that increases in the resting Ca^{2+} level per se are uncoupled from the mechanisms of short-term plasticity. These observations reveal a potential dual role for presynaptic Ca^{2+} stores in giant MFs: a KAR-independent contribution to the maintenance of the low background Ca^{2+} and a KAR-dependent contribution to the use-dependent facilitation of Ca^{2+} transients.

It has been observed that use-dependent enhancement of transmission at MF–CA3 pyramidal cell synapses is substantially stronger than at MF synapses on two types of interneurons (Toth et al., 2000) and is slightly more prominent than that at MF-mossy cell synapses: compare (Lysetskiy et al., 2005) and (Lauri et al., 2003; Scott and Rusakov, 2006). In agreement with this, we found that the PPR of EPSCs evoked by minimal stimulation of MFs in CA3 pyramidal cells is greater than in interneurons (supplemental Table S1, available at www.jneurosci.org as supplemental material). The KAR and Ca^{2+} store mediated facilitation of transmission that is specific to MF–CA3 pyramidal cell synapses could therefore explain, at least partly, the increased probability of CA3 pyramidal cell discharges, as opposed to other MF targets, in response to repetitive afferent firing in this circuitry (Henze et al., 2002).

References

Acsády L, Kamondi A, Sík A, Freund T, Buzsáki G (1998) GABAergic cells are the major postsynaptic targets of mossy fibers in the rat hippocampus. J Neurosci 18:3386–3403.

Alle H, Geiger JR (2006) Combined analog and action potential coding in hippocampal mossy fibers. Science 311:1290–1293.

Alle H, Jonas P, Geiger JR (2001) PTP and LTP at a hippocampal mossy fiber-interneuron synapse. Proc Natl Acad Sci U S A 98:14708–14713.

Bortolotto ZA, Clarke VR, Delany CM, Parry MC, Smolders I, Vignes M, Ho KH, Miu P, Brinton BT, Fantaske R, Ogden A, Gates M, Ornstein PL, Lodge D, Bleakman D, Collingridge GL (1999) Kainate receptors are involved in synaptic plasticity. Nature 402:297–301.

Breustedt J, Schmitz D (2004) Assessing the role of GLUK5 and GLUK6 at hippocampal mossy fiber synapses. J Neurosci 24:10093–10098.

Carter AG, Vogt KE, Foster KA, Regehr WG (2002) Assessing the role of calcium-induced calcium release in short- term presynaptic plasticity at excitatory central synapses. J Neurosci 22:21–28.

Claiborne BJ, Amaral DG, Cowan WM (1986) A light and electron microscopic analysis of the mossy fibers of the rat dentate gyrus. J Comp Neurol 246:435–458.

Contractor A, Swanson G, Heinemann SF (2001) Kainate receptors are involved in short- and long-term plasticity at mossy fiber synapses in the hippocampus. Neuron 29:209–216.

Domenici MR, Berretta N, Cherubini E (1998) Two distinct forms of long-term depression coexist at the mossy fiber-CA3 synapse in the hippocampus during development. Proc Natl Acad Sci U S A 95:8310–8315.

Geiger JR, Jonas P (2000) Dynamic control of presynaptic Ca^{2+} inflow by fast-inactivating K^+ channels in hippocampal mossy fiber boutons. Neuron 28:927–939.

Halasy K, Somogyi P (1993) Subdivisions in the multiple GABAergic innervation of granule cells in the dentate gyrus of the rat hippocampus. Eur J Neurosci 5:411–429.

Henze DA, Buzsáki G (2007) Hilar mossy cells: functional identification and activity in vivo. Prog Brain Res 163:199–216.

Henze DA, Wittner L, Buzsáki G (2002) Single granule cells reliably discharge targets in the hippocampal CA3 network in vivo. Nat Neurosci 5:790–795.

Hirbec H, Francis JC, Lauri SE, Braithwaite SP, Coussen F, Mulle C, Dev KK, Coutinho V, Meyer G, Isaac JT, Collingridge GL, Henley JM, Couthino V (2003) Rapid and differential regulation of AMPA and kainate receptors at hippocampal mossy fibre synapses by PICK1 and GRIP. Neuron 37:625–638.

Jinno S, Kosaka T (2003) Heterogeneous expression of the cholecystokinin-like immunoreactivity in the mouse hippocampus, with special reference to the dorsoventral difference. Neuroscience 122:869–884.

Jonas P, Major G, Sakmann B (1993) Quantal components of unitary EPSCs at the mossy fibre synapse on CA3 pyramidal cells of rat hippocampus. J Physiol 472:615–663.

Kamiya H, Shinozaki H, Yamamoto C (1996) Activation ef metabotropic glutamate receptor type 2/3 suppresses transmission at rat hippocampal mossy fibre synapses. J Physiol 493:447–455.

Kamiya H, Ozawa S, Manabe T (2002) Kainate receptor-dependent short-term plasticity of presynaptic Ca^{2+} influx at the hippocampal mossy fiber synapses. J Neurosci 22:9237–9243.

Kerr AM, Capogna M (2007) Unitary IPSPs enhance hilar mossy cell gain in the rat hippocampus. J Physiol 578:451–470.

Koester HJ, Baur D, Uhl R, Hell SW (1999) Ca^{2+} fluorescence imaging with pico- and femtosecond two-photon excitation: signal and photodamage. Biophys J 77:2226–2236.

Lanthorn TH, Ganong AH, Cotman CW (1984) 2-Amino-4-Phosphonobutyrate Selectively Blocks Mossy Fiber Ca3 Responses in Guinea-Pig But Not Rat Hippocampus. Brain Res 290:174–178.

Lauri SE, Bortolotto ZA, Bleakman D, Ornstein PL, Lodge D, Isaac JT, Collingridge GL (2001) A critical role of a facilitatory presynaptic kainate receptor in mossy fiber LTP. Neuron 32:697–709.

Lauri SE, Bortolotto ZA, Nistico R, Bleakman D, Ornstein PL, Lodge D, Isaac JT, Collingridge GL (2003) A role for Ca^{2+} stores in kainate receptor-dependent synaptic facilitation and LTP at mossy fiber synapses in the hippocampus. Neuron 39:327–341.

Liang Y, Yuan LL, Johnston D, Gray R (2002) Calcium signaling at single mossy fiber presynaptic terminals in the rat hippocampus. J Neurophysiol 87:1132–1137.

Lysetskiy M, Földy C, Soltesz I (2005) Long- and short-term plasticity at mossy fiber synapses on mossy cells in the rat dentate gyrus. Hippocampus 15:691–696.

Manzoni OJ, Castillo PE, Nicoll RA (1995) Pharmacology of metabotropic glutamate receptors at the mossy fiber synapses of the guinea-pig hippocampus. Neuropharmacology 34:965–971.

Mori M, Abegg MH, Gähwiler BH, Gerber U (2004) A frequency-dependent switch from inhibition to excitation in a hippocampal unitary circuit. Nature 431:453–456.

Nicoll RA, Schmitz D (2005) Synaptic plasticity at hippocampal mossy fibre synapses. Nat Rev Neurosci 6:863–876.

Paternain AV, Morales M, Lerma J (1995) Selective antagonism of AMPA receptors unmasks kainate receptor-mediated responses in hippocampal neurons. Neuron 14:185–189.

Pelkey KA, Topolnik L, Lacaille JC, McBain CJ (2006) Compartmentalized Ca^{2+} channel regulation at divergent mossy-fiber release sites underlies target cell-dependent plasticity. Neuron 52:497–510.

Pinheiro PS, Perrais D, Coussen F, Barhanin J, Bettler B, Mann JR, Malva JO, Heinemann SF, Mulle C (2007) GluR7 is an essential subunit of presynaptic kainate autoreceptors at hippocampal mossy fiber synapses. Proc Natl Acad Sci U S A 104:12181–12186.

Rollenhagen A, Sätzler K, Rodríguez EP, Jonas P, Frotscher M, Lübke JH (2007) Structural determinants of transmission at large hippocampal mossy fiber synapses. J Neurosci 27:10434–10444.

Ruiz A, Fabian-Fine R, Scott R, Walker MC, Rusakov DA, Kullmann DM (2003) GABAA receptors at hippocampal mossy fibers. Neuron 39:961–973.

Rusakov DA, Fine A (2003) Extracellular Ca^{2+} depletion contributes to fast activity-dependent modulation of synaptic transmission in the brain. Neuron 37:287–297.

Rusakov DA, Saitow F, Lehre KP, Konishi S (2005) Modulation of presynaptic Ca^{2+} entry by AMPA receptors at individual GABAergic synapses in the cerebellum. J Neurosci 25:4930–4940.

Schmitz D, Mellor J, Nicoll RA (2001) Presynaptic kainate receptor mediation of frequency facilitation at hippocampal mossy fiber synapses. Science 291:1972–1976.

Schmitz D, Mellor J, Breustedt J, Nicoll RA (2003) Presynaptic kainate receptors impart an associative property to hippocampal mossy fiber long-term potentiation. Nat Neurosci 6:1058–1063.

Schoepp DD, Jane DE, Monn JA (1999) Pharmacological agents acting at subtypes of metabotropic glutamate receptors. Neuropharmacology 38:1431–1476.

Scott R, Rusakov DA (2006) Main determinants of presynaptic Ca^{2+} dynamics at individual mossy fiber-CA3 pyramidal cell synapses. J Neurosci 26:7071–7081.

Scott R, Ruiz A, Henneberger C, Kullmann DM, Rusakov DA (2008) Analog modulation of mossy fiber transmission is uncoupled from changes in presynaptic Ca^{2+}. J Neurosci 28:7765–7773.

Shigemoto R, Kinoshita A, Wada E, Nomura S, Ohishi H, Takada M, Flor PJ, Neki A, Abe T, Nakanishi S, Mizuno N (1997) Differential presynaptic localization of metabotropic glutamate receptor subtypes in the rat hippocampus. J Neurosci 17:7503–7522.

Shimizu H, Fukaya M, Yamasaki M, Watanabe M, Manabe T, Kamiya H (2008) Use-dependent amplification of presynaptic Ca^{2+} signaling by axonal ryanodine receptors at the hippocampal mossy fiber synapse. Proc Natl Acad Sci U S A 105:11998–12003.

Simmons PJ (2002) Presynaptic depolarization rate controls transmission at an invertebrate synapse. Neuron 35:749–758.

Smolders I, Bortolotto ZA, Clarke VR, Warre R, Khan GM, O'Neill MJ, Ornstein PL, Bleakman D, Ogden A, Weiss B, Stables JP, Ho KH, Ebinger G, Collingridge GL, Lodge D, Michotte Y (2002) Antagonists of GLU(K5)-containing kainate receptors prevent pilocarpine-induced limbic seizures. Nat Neurosci 5:796–804.

Toth K, Suares G, Lawrence JJ, Philips-Tansey E, McBain CJ (2000) Differential mechanisms of transmission at three types of mossy fiber synapse. J Neurosci 20:8279–8289.

Verkhratsky A (2005) Physiology and pathophysiology of the calcium store in the endoplasmic reticulum of neurons. Physiol Rev 85:201–279.

Weisskopf MG, Zalutsky RA, Nicoll RA (1993) The opioid peptide dynorphin mediates heterosynaptic depression of hippocampal mossy fiber synapses and modulates long-term potentiation. Nature 362:423–427.